A&A 650, A23 (2021)
https://doi.org/10.1051/0004-6361/202039299

Astronomy & Astrophysics

Parker Solar Probe: Ushering a new frontier in space exploration

Special issue

Parker Solar Probe observations of He/H abundance variations in SEP events inside 0.5 au*

C. M. S. Cohen[1], E. R. Christian[2], A. C. Cummings[1], A. J. Davis[1], M. I. Desai[3], G. A. de Nolfo[2], J. Giacalone[4], M. E. Hill[5], C. J. Joyce[6], A. W. Labrador[1], R. A. Leske[1], W. H. Matthaeus[7], D. J. McComas[6], R. L. McNutt Jr.[5], R. A. Mewaldt[1], D. G. Mitchell[5], J. G. Mitchell[2,8], J. S. Rankin[6], E. C. Roelof[5], N. A. Schwadron[9], E. C. Stone[1], J. R. Szalay[6], M. E. Wiedenbeck[10], A. Vourlidas[5], S. D. Bale[11], M. Pulupa[12], and R. J. MacDowall[2]

[1] California Institute of Technology, Pasadena, CA 91125, USA
e-mail: cohen@srl.caltech.edu
[2] NASA/Goddard Space Flight Center, Greenbeelt, MD 20771, USA
[3] University of Texas at San Antonio, San Antonio, TX 78249, USA
[4] University of Arizona, Tucson, AZ 85721, USA
[5] Johns Hopkins University Applied Physics Laboratory, Laurel, MD 20723, USA
[6] Department of Astrophysical Sciences, Princeton University, Princeton, NJ 08544, USA
[7] University of Delaware, Newark, DE 19716, USA
[8] Department of Physics, George Washington University, Washington, DC 20052, USA
[9] University of New Hampshire, Durham, NH 03824, USA
[10] Jet Propulsion Laboratory, California Institute of Technology, Pasadena, CA 91109, USA
[11] Physics Department, University of California at Berkeley, Berkeley, CA 94720, USA
[12] Space Sciences Laboratory, University of California at Berkeley, Berkeley, CA 94720, USA

Received 30 August 2020 / Accepted 1 December 2020

ABSTRACT

Aims. The Parker Solar Probe (PSP) orbit provides an opportunity to study the inner heliosphere at distances closer to the Sun than previously possible. Due to the solar minimum conditions, the initial orbits of PSP yielded only a few solar energetic particle (SEP) events for study. Recently during the fifth orbit, at distances from 0.45 to 0.3 au, the energetic particle suite on PSP, Integrated Science Investigation of the Sun (IS⊙IS), observed a series of six SEP events, adding to the limited number of SEP events studied inside of 0.5 au. Variations in the H and He spectra and the He/H abundance ratio are examined and discussed in relation to the identified solar source regions and activity.

Methods. IS⊙IS measures the energetic particle environment from ∼20 keV to >100 MeV/nuc. Six events were selected using the ∼1 MeV proton intensities, and while small, they were sufficient to calculate proton and helium spectra from ∼1 to ∼10 MeV/nuc. For the three larger events, the He/H ratio as a function of energy was determined. Using the timing of the associated radio bursts, solar sources were identified for each event and the eruptions were examined in extreme ultraviolet emission.

Results. The largest of the selected events has peak ∼1 MeV proton intensities of 3.75 $(\mathrm{cm}^2\ \mathrm{sr\ s\ MeV})^{-1}$. Within uncertainties, the He and H spectra have similar power law forms with indices ranging from −2.3 to −3.3. For the three largest events, the He/H ratios are found to be relatively energy independent; however, the ratios differ substantially with values of 0.0033 ± 0.0013, 0.177 ± 0.047, and 0.016 ± 0.009. An additional compositional variation is evident in both the ^{3}He and electron signatures. These variations are particularly interesting as the three larger events are likely a result of similar eruptions from the same active region.

Key words. Sun: particle emission – Sun: activity – solar-terrestrial relations

1. Introduction

Solar energetic particles (SEPs) have been studied for decades and much progress has been made in understanding their acceleration and transport (see reviews by Reames 1999; Zharkova et al. 2011; Desai & Giacalone 2016; Klein & Dalla 2017, and references therein). However, SEP events exhibit substantial variability in many of their characteristics, including time profiles, composition, and spectral shape, and it is difficult to disentangle the contributions from transport versus acceleration processes when the majority of SEP observations are made near 1 au. Multiple studies have argued that the composition of an SEP event can be attributed to the acceleration process (e.g., Cane et al. 2006), the conditions under which the acceleration occurs (e.g., Tylka et al. 2005; Mason et al. 1999), and the transport through the inner heliosphere (e.g., Ng et al. 2003; Breneman & Stone 1985) with most agreeing that it is a combination of effects that leads to the observed variability.

Most of these processes are expected to have a dependence on the particle's rigidity. As SEP composition is typically calculated relative to a reference element at common velocities (or equivalently energy/nucleon), a rigidity dependence manifests itself as a charge-to-mass (Q/M) dependence. This dependence has been observed to vary significantly from event to event (see

* Movies associated to Figs. 3 and 8 are only available at https://www.aanda.org

e.g., Breneman & Stone 1985). Complicating the interpretation of this variability is the lack of direct measurements of the ion charge state. Although some observations were made using the SEPICA instrument on ACE, this capability is no longer available. Indirect determinations of the average charge states of heavy ions were possible using the geomagnetic cutoff technique and measurements from instruments on SAMPEX (e.g., Mason et al. 1995), but the mission ended in 2004. An alternative is to calculate charge states based on ionization and recombination models (e.g., Mazzotta et al. 1998) for a given assumed temperature.

Recently Reames (2016) utilized the Mazzotta et al. (1998) model to extract Q/M patterns observed in individual SEP events. Combining this with the measured composition relative to the reference composition obtained by averaging over many SEP events from Reames (2014), he determined the temperature of the source material for each event. It was noted that often He/O did not fit with the Q/M abundance pattern of heavier ions. Given that the charge state of He is +2 for all the temperatures considered, Reames (2017) was motivated to investigate the reference He/O abundance ratio of 57. That work suggests that the reference abundance of He/O, presumably reflecting the source before transport effects, is not static, but it varies from event to event over the range of 40 to 90.

Parker Solar Probe (PSP) provides a new opportunity to examine the characteristics of SEP events at distances significantly closer to the Sun. The clear advantage of observations well inside 1 au is the decreased effects of particle transport. With state-of-the-art instrumentation on board, the composition of SEP events can be examined from ~20 keV/nuc to >100 MeV/nuc. As of August 2020, PSP has completed five orbits around the Sun. Due to solar minimum conditions, only a few SEP events have been observed by PSP since launch in 2018 August (see e.g., McComas et al. 2019; Wiedenbeck et al. 2020; Leske et al. 2020; Joyce et al. 2020; Hill et al. 2020; Giacalone et al. 2020; Mitchell et al. 2020; Schwadron et al. 2020); however, recent data from orbit 5 include a series of six SEP events observed inside 0.5 au, from 2020 May 22–June 1. This paper describes these events, identifies their solar sources, and examines their spectra and composition.

2. Observations

Parker Solar Probe (Fox et al. 2016) was launched on 2018 August 12; through a series of Venus flybys, the perihelion of the orbits will gradually be reduced to reach <10 R_S (<0.047 au) by late 2024. Orbit 5 spanned 2020 April 3 to 2020 August 2, with a perihelion of 29 R_S (0.13 au). During this time the Integrated Science Investigation of the Sun (IS⊙IS, McComas et al. 2016) made observations of energetic particles via the Energetic Particle Instrument-Low (EPI-Lo, Hill et al. 2017) and the Energetic Particle Instrument-High (EPI-Hi, Wiedenbeck et al. 2017). EPI-Lo consists of 80 time-of-flight apertures providing observations of particles from 20 keV/nuc to 1.5 MeV/nuc over 2π steradians. EPI-Hi has three telescopes of stacked solid-state detectors, utilizing the standard dE/dx versus residual energy technique to measure ions from ~1 to >100 MeV/nuc and electrons from ~0.5 to 6 MeV. Two of the three telescopes, Low Energy Telescopes (LETs), cover the lower energies of EPI-Hi; one is double-ended providing oppositely viewing apertures LETA and LETB and the other, LETC, is single-ended with its viewing axis perpendicular to that of LETA. The higher energies are observed by the third telescope, the double-ended High Energy Telescope (HET), whose apertures are referred to as HETA and HETB.

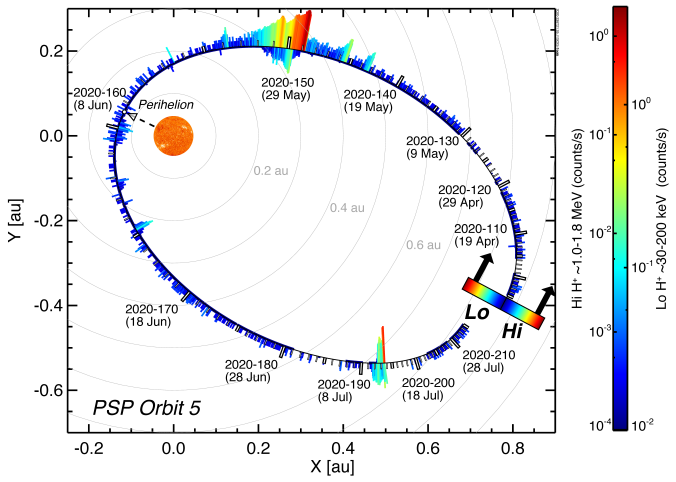

Fig. 1. Geometry of orbit 5 of PSP with overlay of EPI-Hi count rate of LETA range 1 protons (bars extending outside the orbit) corresponding to ~1–2 MeV and EPI-Lo ion count rate summed over all apertures and ~30–200 keV (bars extending inside the orbit). The SEP events of interest are evident in the inbound portion of the orbit inside 0.5 au close to the top of the figure, near day 150. The count rate levels are indicated by both the height and color of the bars.

Figure 1 gives an overview of orbit 5 and the energetic particle measurements. The height and color of the bars on the outside of the orbit correspond to the EPI-Hi LETA rate of protons stopping in the second detector (referred to hereafter as 'range 1' particles, corresponding to ~1–2 MeV protons; see Wiedenbeck et al. 2017), while the height and color of the inside bars indicate the EPI-Lo ~30–200 keV ion observations (summed over all the apertures and dominated by protons). The period of interest is just before perihelion when PSP was at 0.45–0.3 au and is evident as the larger bars colored orange and red for EPI-Hi. A more detailed look at the IS⊙IS observations during the time period is given in Fig. 2 where proton intensities are shown as a function of energy and time (from HETA, top panel; LETA, second panel; and EPI-Lo, third panel), helium intensities (from LETA, fourth panel), and electron count rates (from HETB, bottom panel). The six events are most clearly seen in the LETA proton spectrogram (second panel); the start and stop times for each event are listed in Table 1 along with their peak proton intensities at ~1 MeV.

Not all of the six events are evident in the EPI-Lo and HET data. Clearly events 1, 2, and 6 are too small to extend into the HET energy range. For events 3–5, the HET measurements do not significantly extend the H spectra obtained from LET alone. Events 1–4 are somewhat evident in the EPI-Lo data; however, only event 4 has significant statistics. It may be noted that the apparent onset of event 4 in EPI-Lo does not align with that of EPI-Hi, even when accounting for velocity dispersion. The increase appears to be roughly correlated with a spacecraft roll which complicates the interpretation of the EPI-Lo data. Additionally, the cross calibration between EPI-Lo and EPI-Hi proton measurements has not been fully completed. For these reasons, the analysis presented below focuses on the measurements of LET.

The onsets of the events with the accompanying radio data, showing the presence of type III radio bursts, and magnetic field data are presented in Fig. 3. The top panel shows the hourly

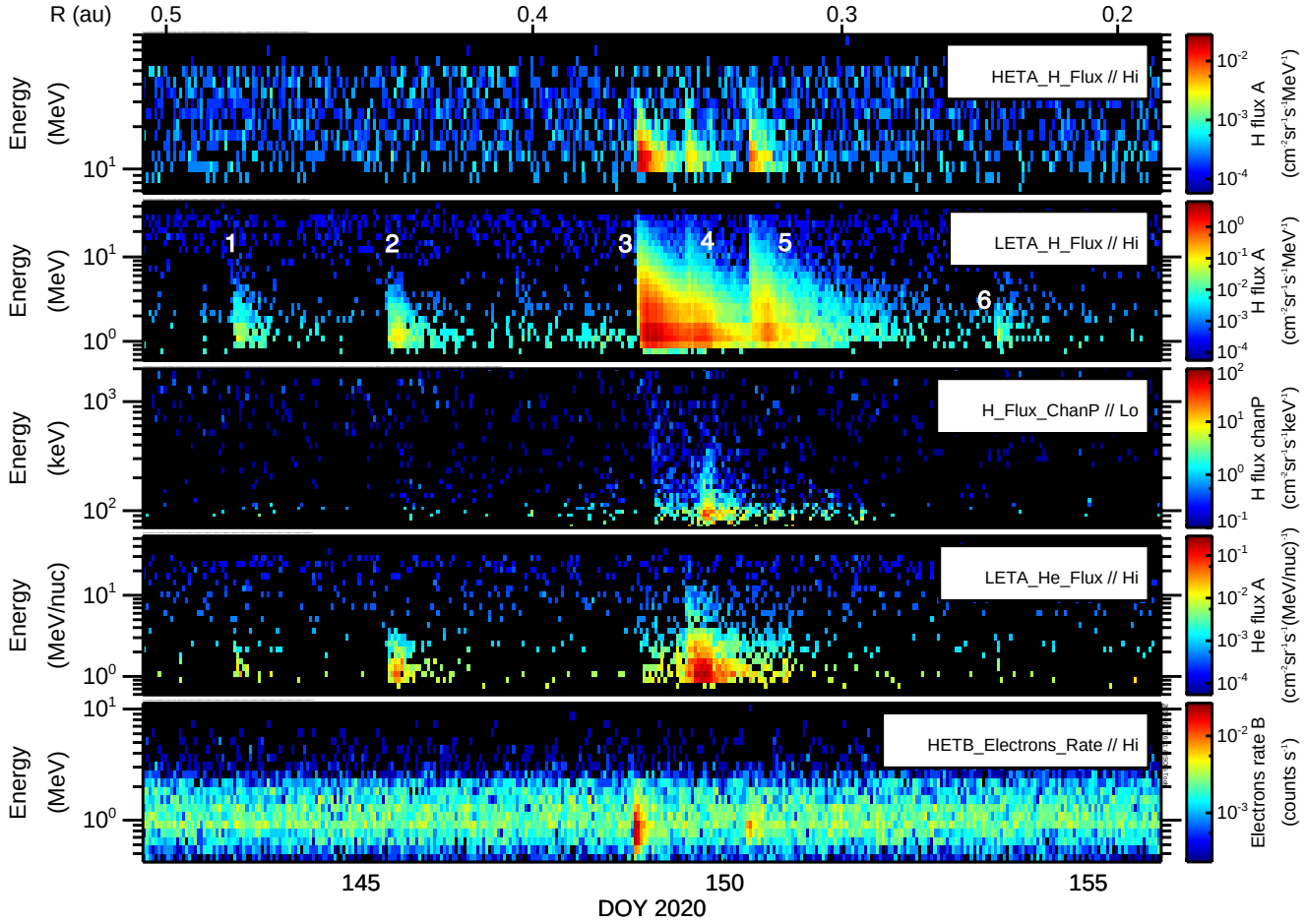

Fig. 2. Spectrograms showing the proton intensity versus energy and time from HETA (*top panel*), LETA (*second panel*), and EPI-Lo (*third panel*); the helium intensity from LETA (*fourth panel*); and the electron count rate from HETB (*bottom panel*). Event numbers are given at the top of the *second panel*.

LETA range 1 proton count rate; the second and third panels show the High Frequency Receiver (HFR) and Low Frequency Receiver (LFR) data from FIELDS Radio Frequency Spectrometer (RFS, Pulupa et al. 2017); the bottom panel displays the RTN components and total magnitude of the magnetic field as measured by FIELDS (Bale et al. 2016), where R points from the Sun to the spacecraft, T is the cross product of the solar rotation axis and R, and N completes the right-handed orthogonal system. Although no significant magnetic field structures are evident, these data are included for completeness. Using the timing of the upper frequencies (~10 MHz) of the radio bursts as a guide, solar source regions and eruptions were determined for each event using Extreme Ultraviolet Imager (EUVI, Wuelser et al. 2003) data from STEREO-A. Images of these regions are displayed in the upper-left insets of Fig. 3 and movies, which more clearly show the eruptions, are available online. Only two of the three active regions involved in the six events were given USAF/NOAA numbers when they rotated onto the Earth-facing hemisphere of the Sun. These region numbers are listed in Table 1.

Clear compositional differences between the six events can be seen qualitatively in Fig. 2. While all six events are evident in the protons, only events 3 and 5 appear to have a clear electron signal at the EPI-Hi energies; although it is not shown, event 4 does have a weak electron signature in EPI-Lo. Event 3 appears to be the strongest in protons, yet, event 4 is the dominant one in He. The differences in events 3–5 are particularly interesting as they all likely originated from the same active region on the Sun and had quite similar eruption signatures; although there are potential complications for event 4, as discussed below.

The mass resolution of EPI-Hi is sufficient to distinguish ^{3}He from ^{4}He (see detailed discussion in Wiedenbeck et al. 2020). Using the event data for range 1 He ions from LETA or LETB with total energies of <8 MeV (i.e., <2 MeV/nuc for ^{4}He and <2.67 MeV/nuc for ^{3}He), the mass distribution of He ions during the six events can be calculated (Fig. 4). Each point in the figure is a single measured ion; the statistics are clearly low for most of the events. Integrating over the event time periods given in Table 1 yields mass histograms shown for events 1, 3, 4, and 5 in Fig. 5. Event 4 (lower-left panel) illustrates the effect of "spillover" from the ^{4}He peak into the ^{3}He peak. The number of ions between mass 2.5 and 3.5 is 40 and between 3.5 and 4.5 is 971, yielding a count ratio of 0.041. This is similar to the amount of spillover observed in STEREO/LET in large events with no measurable ^{3}He signal (see Wiedenbeck et al. 2020). Using this event as a template for one with no "true" ^{3}He signal, it was scaled and compared to the histograms measured in events 1, 3, and 5 in Fig. 5. The scaling factor for a given event is the ratio of the histogram area between mass 3.5 and 4.5 in event 4 to this area in the particular event; these factors are listed in the corresponding panels legends. From this comparison, it appears that event 1 is ^{3}He-rich and that events 3 and 5 have some ^{3}He

Table 1. Parameters of selected events.

Evt #	SEP times [a]	Radio time [b]	H peak intensity [c]	H spectral index	He spectral index	He/H	e-sign.	AR #	CME speed (km s^{-1}) [d]
1	5/22 06–5/22 19	5/22 0420	0.091	−3.2 ± 0.1	−4.1 ± 0.99		No	N/A [e]	–
2	5/24 08–5/25 05	N/A	0.12	−3.3 ± 0.03	−3.3 ± 0.13		No	N/A [e]	(231)
3	5/27 18–5/28 11	5/27 1800	3.75	−2.7 ± 0.001	−3.0 ± 0.68	0.0033 ± 0.0013	Yes	12 764	530 (454)
4	5/28 11–5/29 08	5/28 1020	1.13	−2.4 ± 0.001	−2.7 ± 0.008	0.176 ± 0.047	No	12 764	723
5	5/29 08–5/30 22	5/29 0720	0.56	−2.3 ± 0.001	−2.4 ± 0.069	0.016 ± 0.009	Yes	12 764	–
6	6/1 16–6/2 00	6/1 1630	0.049	−2.9 ± 0.027			No	12 765	(277)
L20 [f]	4/4 02–4/4 18	4/4 0240+	0.9	−4.36 ± 0.06	−4.21 ± 0.26	0.052 ± 0.002		12 738	
W20a [g]	4/20 14–4/20 18	4/20 0042	2.07	−3.6	−4.8		Yes	12 738	
W20b [g]	4/21 12–4/21 18	4/20 0326	11.4	−2.8	−3.6		Yes	12 738	

Notes. [a]Integration times for fluence spectra, month/day hour of 2020 for events 1–6, 2019 for those of Leske et al. (2020, L20) and Wiedenbeck et al. (2020, W20a and W20b). [b]Time at ∼10 MHz to nearest 10 min; no burst was seen for event 2. Multiple bursts from 0240 onwards were noted for L20, [c]at 1.1 MeV in (cm^2 sr s MeV)$^{-1}$, [d]from CACTus using LASCO observations, '–' if not reported; from STEREO-A in parentheses when available, [e]seen by HMI at S25 on the east limb on 2020 May 28, but not assigned an AR#, [f]2019 event described by Leske et al. (2020), [g]2019 events described by Wiedenbeck et al. (2020).

enhancement. Event 2 (not shown) is consistent with no ^{3}He signal and the statistics are too poor to make any conclusions about event 6 (not shown).

Proton and helium spectra are obtained for each event by integrating over the time periods given in Table 1. As the spectra from LETA and LETB are consistent with an isotropic distribution of particles for all of the events, the spectra shown in Fig. 6 are averages of the LETA and LETB spectra; due to thicker windows, LETC spectra begin at a higher energy than LETA and LET B and they were thus not included in the average. A quiet time background spectrum was subtracted from each event spectrum to remove contributions from galactic cosmic rays as well as anomalous cosmic rays for He. Additionally a contribution from the decay of event 3 was subtracted from event 4 (assuming an exponential decay in time) for protons. This primarily affects the energy channels below ∼3 MeV. All the spectra were fairly well fit by power laws and the resulting indices are reported in Table 1; there is modest variation from event to event with the indices ranging from −2.3 to −3.3 for protons. The helium spectral indices are consistent with those of the protons, within uncertainties, except for event 4 where the He spectra is softer than that of protons.

3. Discussion

3.1. Ion spectra and composition

The SEP events of 2020 May–June presented here add to a short list of those observed by PSP. Events measured during previous orbits include the event of 2019 April 4 described by Leske et al. (2020) and the two ^{3}He-rich events of 2019 April 20 and 21 analyzed by Wiedenbeck et al. (2020), all of which occurred while PSP was inside 0.5 au. For comparison, parameters of these three events (identified as L20, W20a, and W20b, respectively) are also given in Table 1. In terms of peak proton intensities, event 3, the largest of this study, falls between the two Wiedenbeck et al. (2020) events, while the event of Leske et al. was smaller and comparable to event 4. The spectra obtained during the 2019 events were also well described by power laws. The indices derived for the 2020 events are closer to those of Wiedenbeck et al. (2020), and are harder than those of Leske; this is even the case for the smallest events from 2020. Wiedenbeck et al. (2020) found He spectra that were softer than those of protons; however, Leske et al. found them comparable. In this regard, the current results more closely follow those of Leske et al. (2020) (in pattern, not in value).

The variability of the strength of the ^{3}He signal is interesting, particularly the fact that event 4 does not have a discernible ^{3}He enhancement while the events preceding and following it, which are from the same active region, appear to have some enhancement. The electron signature has the same pattern, with no signal for event 4 in HET. This may not be surprising as ^{3}He-rich events are also often electron-rich (Cliver 2016, and references therein). The fact that no electron signal is seen in event 1, despite the event being ^{3}He-rich, may be merely a reflection of the size of the event as it is approximately a factor of five smaller than event 5. Ho et al. (2005) suggested that there is a limit to the amount of ^{3}He accelerated in an event, which is likely related

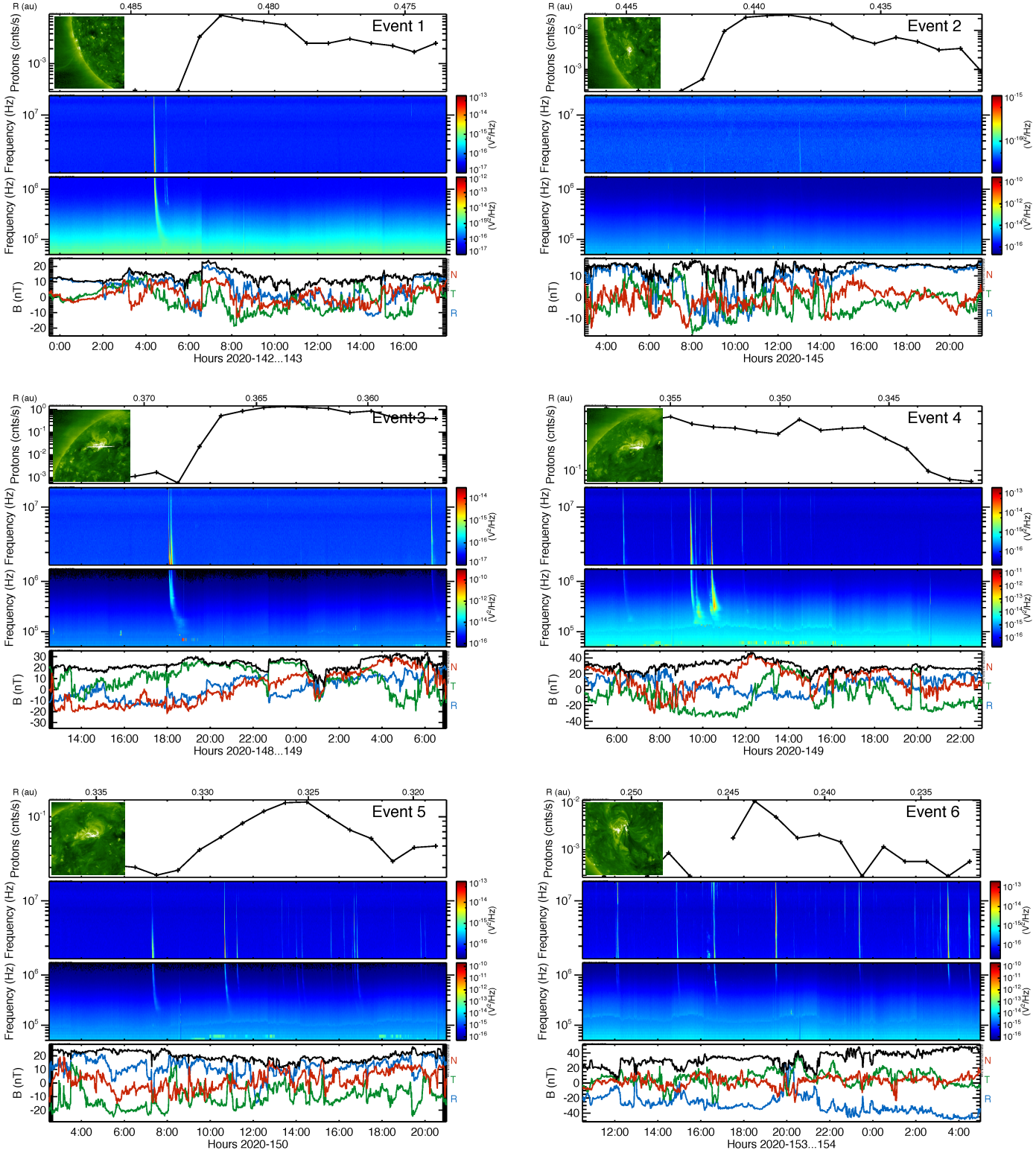

Fig. 3. Onsets of the six events showing the hourly LETA range 1 proton rate in the *top panels*, the HFR and LFR radio data (*second and third panels*), and the magnetic field magnitude (black trace) and *R* (blue trace), *T* (green trace), *N* (red trace) components (*bottom panels*). Insets in the *upper panels* of each event show the solar source region during the related eruption as seen in STEREO-A/EUVI. The images were treated with a wavelet-based algorithm (Stenborg et al. 2008) to enhance the off-limb emission; full movies of the eruptions are available online.

to the size of the region. As events 3, 4, and 5 originated from the same region, it is possible the energetic ^{3}He produced by the region is further depleted in each successive eruption, leading to a decrease in the ^{3}He/^{4}He ratio as a function of time. This would be consistent with the fact that event 3 has enhanced ^{3}He and event 4 does not, but this is inconsistent with the fact that event 5 is also enhanced in ^{3}He. However, Wang et al. (2006) have reported strong variations in the ^{3}He/^{4}He ratio in events

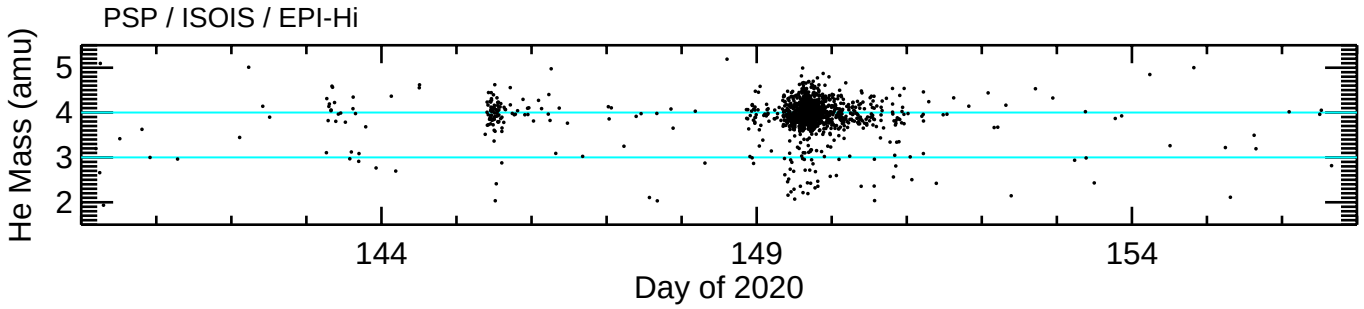

Fig. 4. Calculated masses for detected He ions as a function of time. Each point corresponds to a single range 1 ion with a total energy <8 MeV from LETA or LETB. Blue lines indicate expected locations for ^{3}He and ^{4}He. Events 1–5 are evident as clusters on days 143, 145, 148, 149, and 150, respectively. Event 6 (on day 153) is not clear due to limited statistics.

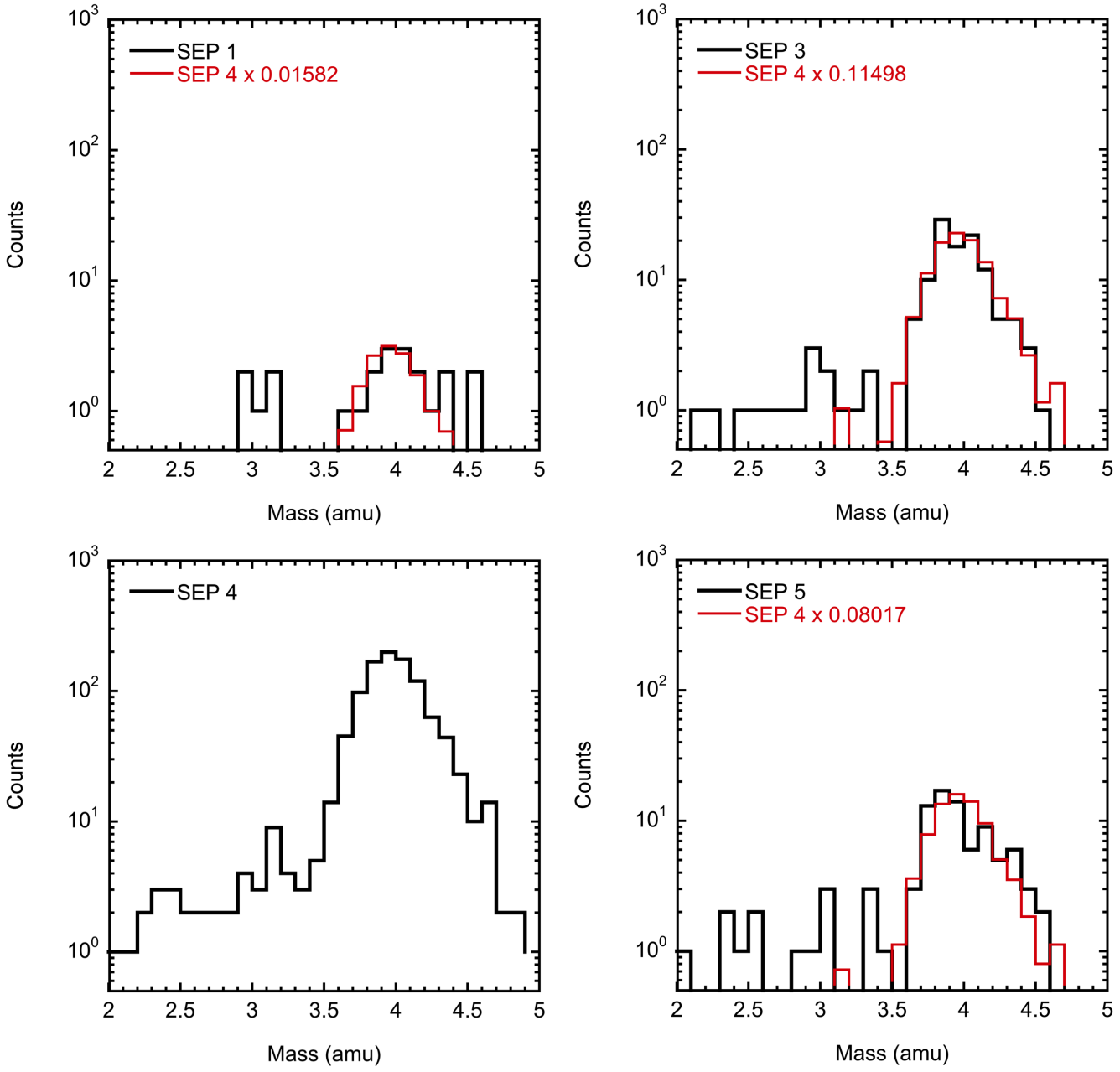

Fig. 5. He mass histograms integrated over the time periods indicated in Table 1 for events 1, 3, 4, and 5. Also shown in red for events 1, 3, and 5 is the event 4 histogram scaled according to the values given in the legends. The distribution of counts in the mass region 2.5–3.5 in event 4 is consistent with spillover from the ^{4}He peak evident in the mass region 3.5–4.5 and not indicative of the presence of ^{3}He. In contrast, the other three events have an excess of counts corresponding to ^{3}He (evident from the comparisons to the scaled event 4 histogram).

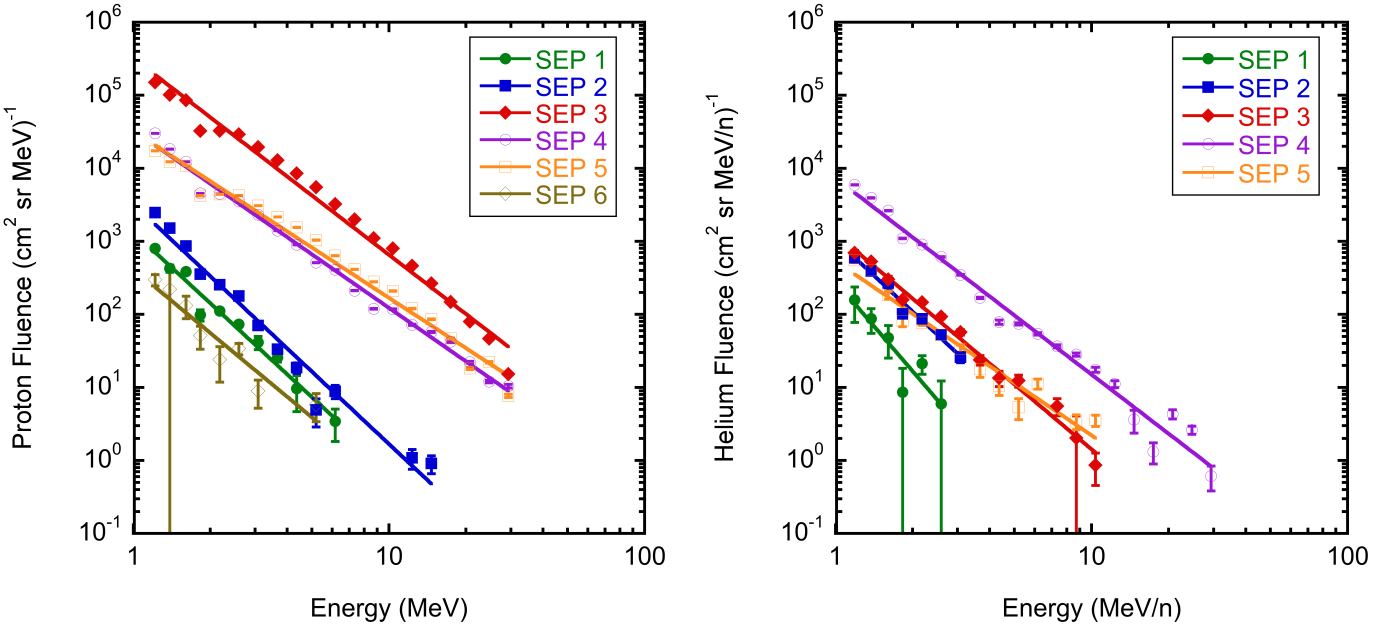

Fig. 6. Event integrated fluence spectra of protons (*left*) and helium (*right*). Lines are power-law fits to the data and uncertainties are statistical. Additional instrumental uncertainties for some points may be as high as 50%.

originating from the same active region with no clear association between the ^{3}He/^{4}He ratios and the characteristics of the eruptions.

This puzzling compositional variation extends to the He/H abundance ratios as well. Event 4 has the largest He/H ratio of 0.177, which is significantly higher than the 0.052 value reported for the Leske et al. (2020) event. Yet, the higher proton fluence and lower He fluence of event 3 results in a very low ratio of 0.0033 and event 5 exhibits a middle value of 0.016. At 1 au, Lario et al. (2003) found significant variations in the He/H ratio in some SEP events, with values ranging from 0.1 at the peak of the event to 0.02 during the declining phase, but not values as low as the 0.0033 ratio observed in event 3. Kallenrode et al. (1992) reported several SEP events observed when Helios was inside of 0.5 au. While they did not calculate He/H abundance ratios, they did tabulate the peak intensities of H and He at 10 MeV/nuc from which a ratio can be determined. The authors separated the events into two categories, impulsive and gradual, according to the duration of the soft X-ray emission. The average He/H ratio for the impulsive group is 0.13 which is consistent with the value of event 4 in this study. However, this is also the event with no detectable ^{3}He, contrary to one of the defining characteristics of events typically associated with impulsive soft X-ray emission. The reported intensities of Kallenrode et al. (1992) for the gradual events result in an average ratio of 0.03, which is significantly higher than that of events 3 and 5, but well below that of event 4.

Recently, Reames (2017) examined the variability of He in a number of large SEP events. He organized the compositional variability of ions from He to Fe according to the charge-to-mass (Q/M) ratio of each ion calculated, assuming an isothermal source and set of reference abundance ratios, which are expected to be typical in the corona. He found that often the enhancement (or depletion) of He/O over the reference ratio of 57 did not follow the same Q/M trend as the heavier ions. Reames was able to obtain better alignment when the reference He/O abundance was allowed to vary from event to event. He concluded that the variation in the He coronal abundance can be substantial and obtained reference He/O ratios of 40–90. Assuming the O/H abundance is 6.25×10^{-4} (as reported in a summary table in Reames 2014), this yields a He/H variability of 0.025 to 0.056, which is not nearly as large a spread as seen in events 3–5 here. It should be noted that the Reames study was for large, shock-accelerated SEP events and may not provide a suitable comparison set for the smaller events studied here.

In a related study, Reames (2019) examined the variability of H/O and also found that to be substantial. Some SEP events were found to have an "excess" of H (relative to the expected enhancement and depletion determined by extrapolating the Q/M power-law dependence to Q/M = 1), independent of the behavior of He/O mentioned above. In some cases the excess was a factor of 10. Such an excess could itself drive the He/H to values of 0.0036 (from the reference value He/H reported in Reames 2014), which is consistent with the He/H ratio obtained for event 3. The expectation is that this increase in H is due to the presence of a shock which is accelerating additional H, but it is not strong enough to accelerate a significant amount of additional heavy ions. It is possible that the ~500 km s^{-1} coronal mass ejection (CME) associated with event 3 could have provided such conditions close to the Sun.

For the larger events, 3–5, the He and H spectra can be used to calculate He/H abundance ratios as a function of energy from ~1 to 10 MeV/nuc (Fig. 7). As is evident in the spectrograms of Fig. 2, there is a substantial variation in the He/H abundances in these three events with a factor of ~50 separating the average He/H ratio of events 3 and 4.

Only in event 4 are there ions heavier than He detected by LET. Unfortunately, the number of range 1 ions measured was ~20 between both LETA and LETB, thus it is not possible to construct a well-defined spectrum. At best, a rough average intensity of O near 2 MeV/nuc can be calculated and compared to that measured for He and H. Such an estimate yields H/O and He/O ratios of ~500 and ~70, respectively. This He/O ratio is close to the nominal value from Reames (2014) of 57 (and well within the range deduced by Reames 2017), but the H/O ratio is approximately a factor of 3 lower than the value from

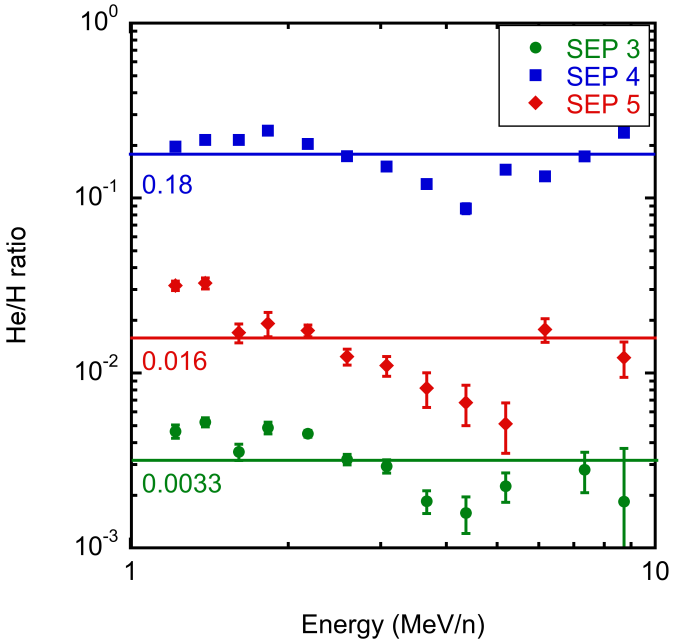

Fig. 7. He/H abundance ratios as a function of energy for events 3, 4, and 5. Lines indicate the average values.

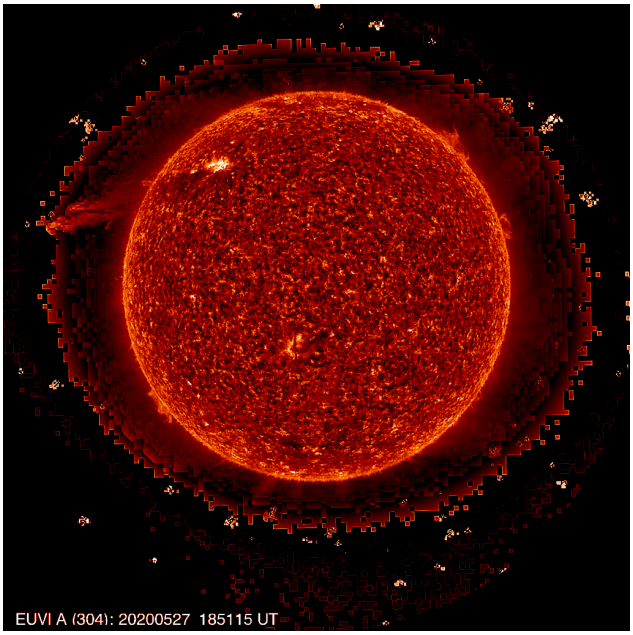

Fig. 8. STEREO-A/EUVI image in 304 Å of erupting cold prominence material (in the north on the east limb) associated with event 3. The image has been treated with a wavelet-based algorithm to enhance the off-limb emission. The corresponding movie is available online.

Reames of 1570. This may be an indication that this event is depleted in H rather than enhanced in He; however, the statistical limitations of the O measurement do not allow for definitive interpretations.

3.2. Solar source regions and eruptions

An initial examination of the solar sources of the six events is best done with STEREO-A data as the spacecraft was well positioned (~70° east of the Earth-Sun line while PSP was ~220°–190° east) to view all the active regions during the ~10 day period studied. Events 1 and 2 originated from the same southern active region, which was not given an active region number by USAF/NOAA. Associated with event 1 are two jet-like (i.e., narrow) ejections (observed at ~04:30 and 05:10), with material appearing to flow along the streamer boundary, and with no obvious associated CME. The eruption associated with event 2 is larger with a faint expanding bubble, increased density at the top of the bubble, and a faint EUV wave (a proxy for the presence of coronal shocks, Patsourakos & Vourlidas 2012) and associated dimming on the eastern side of the active region. A narrow CME with a diffuse front is also observed.

As mentioned previously, the source eruptions of events 3–5 are quite similar. All exhibit brightenings in the EUVI 195 Å channel, an expanding bubble of plasma from the source region (AR 12764), and signatures of an EUV wave. The associated CMEs are relatively narrow, appearing more like wide jets rather than flux ropes, and only event 4 had a faint white-light sheath signature. However, event 4 is complicated by the presence of an eruption an hour before the one at 10:25 in AR 12764. At 09:30 there was activity in another region (AR 12765), behind the southeastern limb (as viewed by STEREO-A), with an accompanying EUV wave and flare ribbons.

This "secondary" active region of event 4 is also the source of event 6. However, this eruption more closely resembles that of event 1, with a small jet of material and no clear EUV bubble or wave. It is very similar to the eruptions related to the events of 2019 April 2–4 as described in Leske et al. (2020) and Kouloumvakos et al. (2020). Overall, the basic difference in the size of the eruptions may explain the difference in size of the six SEP events; however, it is not clear how it relates to the compositional differences.

While it is not entirely clear whether the strong variation in He/H between events 3–5 is a result of the solar source or eruption characteristics, an examination of the amount of cold material being ejected during the eruptions may provide some information. The eruption connected with event 3 is much stronger in EUV than that of event 5, showing more dimming, all of which is on the eastern side of the active region. Additionally, 304 Å (HeII emission) observations show large amounts of cold material being expelled during event 3 (Fig. 8), whereas there is no signature of prominence material ejected in event 5. This is seemingly at odds with the fact that the He/H ratio in event 5 is nearly a factor of 5 higher than that of event 3. Clearly explaining the compositional variations will require more detailed study.

The automated list of CMEs generated by CACTus (Computer Aided CME Tracking, Robbrecht & Berghmans 2004) for both the SOHO/LASCO and STEREO/COR data were examined for white light CMEs associated with these events. The speeds of the best candidates are listed in Table 1. No suitable candidates were found for events 1 and 5. Only events 3 and 4 have CMEs with speeds >500 km s^{-1} (as determined from the LASCO data), with event 4 having the fastest CME. It is possible that this faster CME drives a shock or at least creates a compression region capable of accelerating particles which leads to more energetic ^{4}He, depressing the ^{3}He/^{4}He ratio, an effect that is not present (or is significantly weaker) for the preceding and following events (3 and 5). However, the same argument would suggest more H should be present in event 4, contrary to the observation that event 3 is largest in H fluence (and peak intensity), while event 4 is the largest in He.

One last oddity in the solar signatures is the lack of a radio burst signal associated with event 2. This event is similar in size

(in protons) to event 1 for which there is a clear type III radio burst. Additionally, the two events share the same source region, suggesting that if a radio burst is associated with the second event, PSP/FIELDS should have measured it.

4. Summary

PSP/IS⊙IS observed a series of six SEP events in 2020 May–June during its fifth orbit around the Sun. These events add to the increasing catalog of events observed inside 0.5 au. Source regions and eruptions for all the events have been identified; surprisingly even with similar eruption signatures from the same source region, SEP events with a significantly different composition can result. The fact that many of the events have EUV waves, even when the coronagraph CME signatures are weak, implies the particle acceleration may be occurring very low in the corona and early in the eruption process. The events have power law spectra that are similar in slope to SEP events measured by IS⊙IS in orbit 2 (2019 April), but their He/H abundance ratios show dramatic variations. There is also evidence of significant differences in the ^{3}He/^{4}He ratios, despite limited statistics. The largest of the six events is still smaller than the largest seen in orbit 2 (in ∼1 MeV protons); however, with the recent increase in solar activity, it is likely that more and larger SEP events will be measured by IS⊙IS in the future. With larger events, studies of ions heavier than He will be possible and provide additional clues regarding the acceleration processes involved.

Acknowledgements. This work was supported by NASA's Parker Solar Probe Mission, contract NNN06AA01C. Parker Solar Probe was designed, built, and is now operated by the Johns Hopkins Applied Physics Laboratory as part of NASA's Living with a Star (LWS) program. Support from the LWS management and technical team has played a critical role in the success of the Parker Solar Probe mission. We thank all the scientists and engineers who have worked hard to make PSP a successful mission. In particular, we thank B. Kecman, W. R. Cook and J. Burnham, without whom the EPI-Hi instrument would not be possible. S.D.B. acknowledges support of the Leverhulme Trust Visiting Professorship program. A.V. acknowledges support from NASA grants 80NSSC19K1261 and 80NSSC19K0069. The Sun Earth Connection Coronal and Heliospheric Investigation (SECCHI) was produced by an international consortium of the Naval Research Laboratory (USA), Lockheed Martin Solar and Astrophysics Lab (USA), NASA Goddard Space Flight Center (USA), Rutherford Appleton Laboratory (UK), University of Birmingham (UK), Max Planck Institute for Solar System Research (Germany), Centre Spatiale de Liège (Belgium), Institut d'Optique Theorique et Appliquée (France), and Institut d'Astrophysique Spatiale (France). STEREO data are available for download at https://secchi.nrl.navy.mil/. This paper uses data from the CACTus CME catalog, generated and maintained by the SIDC at the Royal Observatory of Belgium. The IS⊙IS data and visualization tools are available to the community at https://spacephysics.princeton.edu/missions-instruments/isois; data are also available via the NASA Space Physics Data Facility (https://spdf.gsfc.nasa.gov/).

References

Bale, S. D., Goetz, K., Harvey, P. R., et al. 2016, Space Sci. Rev., 204, 49
Breneman, H. H., & Stone, E. C. 1985, ApJ, 299, L57
Cane, H. V., Mewaldt, R. A., Cohen, C. M. S., & von Rosenvinge, T. T. 2006, J. Geophys. Res., 111, A06S90
Cliver, E. W. 2016, ApJ, 832, 128
Desai, M., & Giacalone, J. 2016, Liv. Rev. Sol. Phys., 13, 3
Fox, N. J., Velli, M. C., Bale, S. D., et al. 2016, Space Sci. Rev., 204, 7
Giacalone, J., Mitchell, D. G., Allen, R. C., et al. 2020, ApJS, 246, 29
Hill, M. E., Mitchell, D. G., Andrews, G. B., et al. 2017, J. Geophys. Res. Space Phys., 122, 1513
Hill, M. E., Mitchell, D. G., Allen, R. C., et al. 2020, ApJS, 246, 65
Ho, G. C., Roelof, E. C., & Mason, G. M. 2005, ApJ, 621, L141
Joyce, C. J., McComas, D. J., Christian, E. R., et al. 2020, ApJS, 246, 41
Kallenrode, M.-B., Cliver, E. W., & Wibberenz, G. 1992, ApJ, 391, 370
Klein, K.-L., & Dalla, S. 2017, Space Sci. Rev., 212, 1107
Kouloumvakos, A., Vourlidas, A., Rouillard, A. P., et al. 2020, ApJ, 899, 107
Lario, D., Roelof, E. C., Decker, R. B., et al. 2003, Ann. Geophys., 21, 1229
Leske, R. A., Christian, E. R., Cohen, C. M. S., et al. 2020, ApJS, 246, 35
Mason, G. M., Mazur, J. E., Looper, M. D., & Mewaldt, R. A. 1995, ApJ, 452, 901
Mason, G. M., Cohen, C. M. S., Cummings, A. C., et al. 1999, Geophys. Res. Lett., 26, 141
Mazzotta, P., Mazzitelli, G., Colafrancesco, S., & Vittorio, N. 1998, A&AS, 133, 403
McComas, D. J., Alexander, N., Angold, N., et al. 2016, Space Sci. Rev., 204, 187
McComas, D. J., Christian, E. R., Cohen, C. M. S., et al. 2019, Nature, 576, 223
Mitchell, D. G., Giacalone, J., Allen, R. C., et al. 2020, ApJS, 246, 59
Ng, C. K., Reames, D. V., & Tylka, A. J. 2003, ApJ, 591, 461
Patsourakos, S., & Vourlidas, A. 2012, Sol. Phys., 281, 187
Pulupa, M., Bale, S. D., Bonnell, J. W., et al. 2017, J. Geophys. Res. Space Phys., 122, 2836
Reames, D. V. 1999, Space Sci. Rev., 90, 413
Reames, D. V. 2014, Sol. Phys., 289, 977
Reames, D. V. 2016, Sol. Phys., 291, 911
Reames, D. V. 2017, Sol. Phys., 292, 156
Reames, D. V. 2019, Sol. Phys., 294, 69
Robbrecht, E., & Berghmans, D. 2004, A&A, 425, 1097
Schwadron, N. A., Bale, S., Bonnell, J., et al. 2020, ApJS, 246, 33
Stenborg, G., Vourlidas, A., & Howard, R. A. 2008, ApJ, 674, 1201
Tylka, A. J., Cohen, C. M. S., Dietrich, W. F., et al. 2005, ApJ, 625, 474
Wang, Y. M., Pick, M., & Mason, G. M. 2006, ApJ, 639, 495
Wiedenbeck, M. E., Angold, N. G., Birdwell, B., et al. 2017, PoS(ICRC2017)016, 35, 16
Wiedenbeck, M. E., Bucik, R., Mason, G. M., et al. 2020, ApJS, 246, 42
Wuelser, J.-P., Lemen, J. R., Tarbell, T. D., et al. 2003, SPIE, 111
Zharkova, V. V., Arzner, K., Benz, A. O., et al. 2011, Space Sci. Rev., 159, 357